

# Partially Absorbed Comptonization Spectrum from the Nearly Edge-on Source X 1822–371

R. Iaria<sup>1</sup>, T. Di Salvo<sup>2,1</sup>, L. Burderi<sup>3</sup>, N. R. Robba<sup>1</sup>

iaria@gifco.fisica.unipa.it

## ABSTRACT

We report the results of a spectral analysis over the range 0.1–200 keV performed on the dipping source X 1822–371 observed by BeppoSAX. We find the best fit to the continuum using a partially covered Comptonization model, due to scattering off soft seed photons by electrons at a temperature of  $\sim 4.8$  keV, without the presence of any soft blackbody emission. The equivalent hydrogen column obtained for the absorbed component is  $\sim 4.5 \times 10^{22}$  cm<sup>-2</sup>, an order of magnitude larger than the Galactic absorption for this source, and the covering fraction is  $\sim 71\%$ . Because the inclination angle of X 1822–371 to the line of sight is  $\sim 85^\circ$ , this model gives a reasonable scenario for the source: the Comptonized spectrum could come from an extended accretion disk corona (ADC), probably the only region that can be directly observed due to the high inclination. The excess of matter producing the partial covering could be close to the equatorial plane of the system, above the outer disk, occulting the emission from the inner disk and the inner part of the ADC.

An iron emission line is also present at  $\sim 6.5$  keV with an equivalent width of  $\sim 150$  eV. We argue that this strong iron line cannot be explained as reflection of the Comptonized spectrum by the accretion disk. It is probably produced in the ADC. An emission line at  $\sim 1.9$  keV (with an equivalent width of  $\sim 54$  eV) and an absorption edge at  $\sim 8.7$  keV (with an optical depth of  $\sim 0.1$ ) are also required to fit this spectrum. These features are probably produced by highly ionized iron (Fe XXIV) present in the outer part of the ADC, where the plasma density is  $\sim 10^{11} - 10^{12}$  cm<sup>-3</sup> and ionized plasma is present.

*Subject headings:* stars: individual: X 1822–371 — stars: neutron stars — X-ray: stars — X-ray: spectrum — X-ray: general

---

<sup>1</sup>Dipartimento di Scienze Fisiche ed Astronomiche, Università di Palermo, via Archirafi n.36, 90123 Palermo, Italy

<sup>2</sup>Astronomical Institute “Anton Pannekoek,” University of Amsterdam and Center for High-Energy Astrophysics, Kruislaan 403, NL 1098 SJ Amsterdam, the Netherlands

<sup>3</sup>Osservatorio Astronomico di Roma, Via Frascati 33, 00040 Monteporzio Catone (Roma), Italy

## 1. Introduction

Low Mass X-ray Binaries (LMXB) consist of a low mass star ( $M \leq 1 M_{\odot}$ ) and a neutron star (NS), generally with a weak magnetic field ( $B \leq 10^{10}$  Gauss). In these systems the X-ray source is powered by accretion of mass overflowing the Roche lobe of the companion star and forming an accretion disk around the NS. Different inclinations of the line of sight with respect to the orbital plane can explain the different characteristics of the light curve observed in these systems. At low inclinations eclipses and dips will not be visible in the light curves, while they can be present at high inclinations. About 10 LMXBs are known to show periodic dips in their X-ray light curves. The dip intensities, lengths and shapes change from source to source, and, for the same source, from cycle to cycle. Dips are probably due to a thicker region in the outer rim of the accretion disk, formed by the impact with the disk of the gas stream from the Roche-lobe filling companion star. For systems seen almost edge-on, X-ray emission is still visible due to the presence of an extended accretion disk corona (ADC, see White & Holt, 1982) which can be periodically eclipsed by the companion star.

X 1822–371 is a LMXB seen almost edge-on, with an inclination angle  $i \sim 85^{\circ}$  (Hellier & Mason, 1989). Its light curve shows both dips and eclipses of the X-ray source by the companion star. The partial nature of the eclipse indicates that the X-ray emitting region is extended, and that the observed X-rays are scattered in an ADC. The 1-10 keV spectrum of X 1822–371 as observed by EXOSAT was fitted by an absorbed blackbody plus a power-law component, with an iron emission line at  $\sim 6.7$  keV (Hellier and Mason, 1989). The 1-30 keV spectrum observed by *Ginga* could not be described by the model above, that gave a reduced  $\chi^2$  of 12 (Hellier, Mason and Williams, 1992), probably for the better statistics and the wider energy range of *Ginga* with respect to EXOSAT. Other combinations of power-law, blackbody and thermal bremsstrahlung were used to fit these data, but none of these models gave an acceptable fit. Heinz & Nowak (2001) analysed simultaneous observations with RXTE and ASCA of X 1822–371. They showed that both the source spectrum and light curve can be well fitted by two models, representing the case of an optically thick and an optically thin corona, respectively. In the first case, no soft thermal component from the inner region contributes to the source spectrum and the emission from the corona is described by a cutoff power law partially absorbed by a cold atmosphere above the disk. In the second case the model consists of a blackbody component, emitted from the central source and scattered into the line of sight by the optically thin corona, and a cutoff power law emitted by the corona. Both this models could well describe the data, and therefore it was not possible to distinguish between them.

Recently this source was studied by Parmar et al. (2000) using data from the BeppoSAX satellite in the energy range 0.3–40 keV. They fit the spectrum using a Comptonization model, with a seed-photon temperature of  $\sim 0.1$  keV, an electron temperature of  $\sim 4.5$  keV, and a Comptonizing cloud optical depth of  $\tau \sim 26$ , plus a strong blackbody component, at the temperature of  $\sim 1.9$  keV, which contributes more than 40% of the 0.3–40 keV flux of the source. An emission line at  $\sim 6.5$  keV and an absorption edge at  $\sim 1.3$  keV were also present. We have analysed the same data

using the whole BeppoSAX range (0.1–200 keV). We confirm that the model used by Parmar et al. (2000) can well fit the X 1822–371 spectrum, but we find a better fit using a Comptonization model with partial covering, two emission lines, at  $\sim 6.5$  keV and  $\sim 1.9$  keV, respectively, and an absorption edge at  $\sim 8.7$  keV. In our model there is no need of a blackbody emission or an absorption edge at low energy.

## 2. Observations and Spectral Analysis

The Narrow Field Instruments (NFI) on board BeppoSAX satellite (Boella et al. 1997) observed X 1822–371 on 1997 September 9 and 10, for an effective exposure time of  $\sim 43$  ks. The NFIs are four co-aligned instruments which cover more than three decades of energy, from 0.1 keV up to 200 keV, with good spectral resolution in the whole range. The Low Energy Concentrator/Spectrometer (LECS) operating in the range 0.1–10 keV and the Medium Energy Concentrator/Spectrometer (MECS, 1–11 keV) have imaging capabilities with field of view of  $20'$  and  $30'$  radius, respectively. We selected data for scientific analysis in circular regions, centered on the source, of  $8'$  and  $4'$  radii for LECS and MECS, respectively. The background subtraction was obtained using blank sky observations in which we extracted the background spectra in regions of the field of view similar to those used for the source. The High Pressure Gas Scintillation Proportional Counter (HPGSPC, 7–60 keV) and the Phoswich Detection System (PDS, 13–200 keV) are non-imaging instruments, because their field of views, of  $\sim 1^\circ$  FWHM, are delimited by collimators. In the spectral analysis we used the standard energy ranges for the NFIs, that are: 0.12–4 keV for the LECS, 1.8–10 keV for the MECS, 7–30 keV for the HPGSPC and 15–200 keV for the PDS. As customary, in the spectral fitting procedure we allowed for different normalizations in the LECS, HPGSPC and PDS spectra relative to the MECS spectrum, and checked *a posteriori* that derived values are in the standard range for each instrument. We rebinned the energy spectra in order to have at least 30 counts/channel. The LECS and MECS spectra were furtherly rebinned in order to oversample the full width at half maximum of the energy resolution by a factor of 5 in the whole energy range.<sup>4</sup>

The observed average unabsorbed flux of the source in the 0.1–100 keV energy range is  $1.55 \times 10^{-9}$  ergs  $\text{cm}^{-2}$   $\text{s}^{-1}$ . Adopting a distance of 2.5 kpc (Mason & Cordova, 1982), it corresponds to an unabsorbed luminosity of  $1.15 \times 10^{36}$  ergs/s. This is compatible with the previously reported isotropic luminosity of the X-ray source of  $\sim 10^{36}$  ergs/s (Mason & Cordova, 1982).

In Figure 1 (upper panel) we plotted the X 1822–371 light curve in the energy bands 1.8–10.5 keV (MECS data) versus the orbital phase (using the orbital period reported in Parmar et al. 2000). In the light curve a sinusoidal variation and a partial eclipse at the orbital phase of  $\sim 0.8$  are present. The hardness ratio (the ratio between the counts in the two energy bands 4–8 keV

---

<sup>4</sup>see the BeppoSAX cookbook at <http://www.sdc.asi.it/software/index.html>

and 1–4 keV, lower panel in Fig. 1) does not show large variations. Therefore we performed our spectral analysis on the source spectrum averaged over the whole orbital phase.

We fitted the model obtained by Parmar et al. (2000) in the energy range 0.3–40 keV, to the BeppoSAX data in the energy range 0.12–200 keV. The model consists of photoelectric absorption by cold matter, a blackbody (BB), a Comptonized component (hereafter *Comptt*, Titarchuk 1994), an emission line at  $\sim 6.5$  keV and an absorption edge at  $\sim 1.3$  keV. We obtained a  $\chi^2/d.o.f. = 245/201$ . The values of the parameters are compatible with the values obtained in the range 0.3–40 keV (Parmar et al., 2000) and are reported in Table 1 (Model 1). This model, however, presents two characteristics that, in our opinion, are hard to explain, i.e. the amount of photoelectric absorption,  $N_H$ , and the luminosity of the blackbody component. The value of  $N_H$  reported in Parmar et al. (2000) is  $\sim 1.2 \times 10^{20} \text{ cm}^{-2}$ , an order of magnitude lower than the Galactic absorption expected in the direction of this source (see §3). Using the whole BeppoSAX energy range, we find a larger value  $N_H \sim 6 \times 10^{20} \text{ cm}^{-2}$ , that is still smaller (by a factor of 1.7) than the expected value. Again a very low value of photoelectric absorption is found in the RXTE and ASCA data when the optically thin corona model (consisting of blackbody and cutoff power law) is used (Heinz & Nowak 2001). Moreover, the blackbody component in this model contributes more than 40% of the total source luminosity, that is quite large considering that the source is seen almost edge-on. Both these points were already noted and discussed by Parmar et al. (2000).

We were therefore motivated to search for another model that could both best fit the data and have a simple physical interpretation. Then we repeated the analysis trying several models. In particular given that the source is seen almost edge-on, we tried a Comptonization model (*Compst*, Sunyaev & Titarchuk, 1980) with partial covering and an emission line at  $\sim 6.5$  keV. In this way, we obtained a  $\chi^2/d.o.f. = 291/204$ ; the corresponding values of the parameters are reported in Table 1 (Model 2). In Figure 2 (upper panel) we present the BeppoSAX broad band spectrum and Model 2, and in the same figure (middle panel) we show the residuals in units of  $\sigma$  with respect to Model 2. In the residuals an emission feature at  $\sim 2$  keV and an absorption feature at  $\sim 10$  keV are present. These residuals are of the order of 6 – 8% at 2 keV and of 5% at 10 keV, much higher than any systematic residuals in the MECS and HPGSPC data with respect to the Crab spectrum.<sup>5</sup> Therefore we firstly added an emission line at  $\sim 1.9$  keV, which significantly improved the fit. We obtained a  $\chi^2/d.o.f. = 236/201$ , obtaining a probability of chance improvement of the fit (with respect to Model 2) of  $\sim 3.61 \times 10^{-9}$ . Then we added an absorption edge at  $\sim 8.7$  keV, obtaining a  $\chi^2/d.o.f. = 206/199$ , and a probability of chance improvement of the fit (with respect to the previous model) of  $\sim 3.51 \times 10^{-5}$ . These two features fall at the ends of the MECS energy range. We note that no problems are known to exist in the MECS response matrix at the ends of the energy range and the MECS spectra of many sources as bright as X 1822–371 (or even brighter) have been published without any need of features at 2 keV or 8 keV. However, we wanted to be sure that such features could not be due to instrumental systematics. Using a reduced energy

---

<sup>5</sup>see the BeppoSAX cookbook at the web site <http://www.asdc.asi.it/bepposax/software/index.html>.

range for the MECS (3–8 keV) these features are still statistically significant, giving probabilities of chance improvement of the fit of  $\sim 5 \times 10^{-3}$  and  $\sim 1.8 \times 10^{-5}$  for the low-energy line and the absorption edge, respectively. We also tried to fit the BeppoSAX spectrum using the whole MECS range (1.8–10 keV) and ignoring all the HPGSPC points below 10 keV. Again the addition of the edge at 8.5 keV was statistically significant ( $\sim 10^{-5}$ ) demonstrating that this feature is present in both the MECS and the HPGSPC data. We therefore conclude that these features, which are also expected to be emitted in photo-ionized ADCs (e.g. Ko & Kallman 1994; Kallman et al. 1996), are most probably real and not instrumental effects.

The values of the parameters corresponding to the best fit model are reported in Table 1 (Model 3). We plotted in Figure 2 (lower panel) the residuals in unit of  $\sigma$  with respect to Model 3, and in Figure 3 the unfolded spectrum corresponding to this model.

In order to obtain some information about the seed-photon temperature of the Comptonization spectrum we tried the *Comptt* model (Titarchuk, 1994) instead of the *Compst* model. We obtain an equivalently good fit (see Table 1, Model 4). However, because the seed-photon temperature is close to the low energy end of our spectral range, we can only estimate an upper limit to this temperature of  $\sim 0.2$  keV.

To summarize, a brief description of the best fit parameters follows. We obtained a hydrogen equivalent column  $N_H \simeq 1.2 \times 10^{21} \text{ cm}^{-2}$ . The hydrogen equivalent column of the partial covering is  $N_{\text{HPC}} \simeq 4.5 \times 10^{22} \text{ cm}^{-2}$  and the covered region corresponds to a fraction of 71% of the total. The Comptonized component has an electronic temperature of  $kT_e \sim 4.7$  keV and optical depth  $\tau \sim 14$  for a spherical geometry. We find a broad emission line at  $\sim 6.5$  keV, with  $FWHM = 0.70$  keV and equivalent width of  $\sim 150$  eV. An emission line at  $\sim 1.9$  keV, with  $FWHM = 0.27$  keV and equivalent width of  $\sim 54$  eV, and an absorption edge at  $\sim 8.7$  keV, with optical depth  $\tau_{\text{max}} \sim 0.1$ , are also detected with high statistical significance.

### 3. Discussion

We analysed data of the dipping source X 1822–371 from a BeppoSAX 43 ks observation in the energy range 0.1–200 keV. We obtained the best fit to these data using a partial covered Comptonization model, plus two emission lines and an absorption edge. The results of our spectral analysis of X 1822–371 are discussed in the following.

The equivalent absorption column  $N_H$  we obtained is  $\sim 1.2 \times 10^{21} \text{ cm}^{-2}$ . For a distance to the source of 2.5 kpc (Mason & Cordova, 1982) the visual extinction in the direction of X 1822–371 is  $A_v = 0.87 \pm 0.32$  mag (Hakkila et al. 1997). Using the observed correlation between visual extinction and absorption column (Predehl & Schmitt 1995) we find  $N_H = (1.02 \pm 0.02) \times 10^{21} \text{ cm}^{-2}$ , this value is much higher than the value obtained by Parmar et al. (2000) and by using Model 1. On the other hand the expected Galactic absorption is in perfect agreement with the value that we obtained using Model 3 and Model 4. In our model the Comptonization spectrum

is partially absorbed for the presence of an excess of matter close to the source, obscuring part of the emission region. The absorption column of this partial covering is  $\sim 4.5 \times 10^{22} \text{ cm}^{-2}$ , an order of magnitude larger than the Galactic absorption, and covers a fraction of  $\sim 71\%$  of the source spectrum.

The continuum is well fitted by a Comptonization spectrum, probably produced in a hot ( $kT_e \sim 4.7 \text{ keV}$ ) region of moderate optical depth ( $\tau \sim 14$ , for a spherical geometry) probably surrounding the neutron star. Note that in this spectral deconvolution there is no need of a soft blackbody. This component is needed to fit the soft emission of the source when the partial covering is not used, as in Model 1 of Table 1, i.e. the model adopted by Parmar et al. (2000). In this case the measured contribution of the blackbody to the 1–10 keV flux is greater than 40%. In this scenario, as already noted by Parmar et al. (2000), the blackbody component is most probably emitted in the inner part of the system (i.e. from an optically thick boundary layer close to the neutron star surface or from the neutron star itself). It is therefore unlikely to be observed directly in a high inclination ( $\sim 85^\circ$ ) source as X 1822–371. One can suppose that part of the blackbody emission can be scattered into the line of sight by the corona. However, because the optical depth of this corona, as deduced by fitting its spectrum with Comptonization models, is  $\tau \gtrsim 10$  (see Table 1 and Parmar et al. 2000), any blackbody spectrum passing through it will be (almost) completely reprocessed. Then the blackbody should contribute a low percentage of the total source luminosity or should not be present. We believe that a more reasonable scenario is the one proposed by our Model 3 and Model 4, in agreement with the optically thick scenario used by Heinz & Nowak (2001) to fit simultaneous RXTE and ASCA observations.

The Comptonized component probably originates in an ADC that could be formed by evaporation of the outer layers of the disk illuminated by the emission of the central object (White & Holt, 1982). The radius of the corona can be written as  $R_c \simeq (M_{NS}/M_\odot) T_7^{-1} R_\odot$  (White & Holt, 1982), where  $M_{NS}$  is the mass of the compact object,  $M_\odot$  and  $R_\odot$  are mass and radius of the Sun, and  $T_7$  is the ADC temperature in units of  $10^7 \text{ K}$ . Under this hypothesis, using the values reported in Table 1 (Model 3), we find that the radius of the ADC is  $R_c \simeq 1.8 \times 10^5 \text{ km}$ . Similar values for the ADC radius are reported by White & Holt (1982,  $R_c \simeq 2 \times 10^5 \text{ km}$ ) and by Heinz & Nowak (2001,  $R_c \simeq 2.9 \times 10^5 \text{ km}$ ) for X 1822–371. Using the relation  $\tau = \sigma_T N_e R_c$  we can infer the density of the ADC, where  $\tau$  is the optical depth obtained by the fit,  $\sigma_T$  is the Thomson cross-section,  $N_e$  is the number of particles per unit volume and  $R_c$  is the ADC radius calculated above. Note that we are considering  $N_e$  constant along the radius of the corona, that is a rough approximation. Under this hypothesis we find  $N_e \simeq 1.15 \times 10^{15} \text{ cm}^{-3}$ . This value is in line with previous simulations of ADC (Vrtilek et al., 1993). In fact, considering an inclination angle of  $85^\circ$  (i.e. an angle of  $\sim 5^\circ$  from the disk plane), they find a density along the line of sight in the ADC corona of around  $10^{15} \text{ cm}^{-3}$  (see Fig. 2 in Vrtilek et al., 1993). Following Frank et al. (1987) and using the orbital parameters reported by Parmar et al. (2000), we estimated that the accretion disk radius is  $R_d \sim 4.3 \times 10^5 \text{ km}$ , similar to the value  $R_d \simeq 4 \times 10^5 \text{ km}$  obtained by White & Holt (1982). The disk radius is therefore larger than the estimated radius of the ADC, as expected. In particular the ratio between

the accretion disk radius and the coronal radius is  $R_d \simeq 2.4R_c$ .

Our proposed model is also in agreement with the general behavior of high inclination dipping sources (see e.g. Balucinska-Church et al. 2000; Smale et al. 2000, and references therein). The model used to describe their spectra consists of a point-like blackbody emission and a Comptonized component from the ADC. The spectral evolution during the dips, when we observe the source emission through the thickened region of the accretion disk rim, can be described in terms of a “progressive covering” given by an absorber moving progressively across the emission regions. While the blackbody is rapidly absorbed, suggesting that it is emitted by a compact region (probably from the NS), the Comptonized component is partially absorbed, suggesting that its emission region, i.e. the ADC, is extended. In particular in the case of X 1624–490, Smale et al. (2000) showed that the ADC has a larger angular size than the absorber and has a height-to-radius ratio of  $\sim 10\%$ , with an estimated coronal radius of  $\sim 5 \times 10^5$  km (similar to the value we found above for X 1822–371). The spectrum of X 1822–371 is very similar to these dip spectra, with the lack of the blackbody component (that is probably completely absorbed) and a partially covered Comptonized component. Therefore, in this case of very high inclination, we probably always observe the source emission through the thickened accretion disk. The presence of a thickened outer disk is also suggested by the recent *XMM-Newton* results on EXO 0748–67 (Cottam et al. 2001). The presence of a wealth of emission lines and absorption edges in the range between 0.4 and 1 keV, showing no eclipses or other modulations related to the orbital phase and large widths probably due to velocity broadening, suggests that these low-energy features are emitted in a flared accretion disk extending high above the equatorial plane (Cottam et al. 2001).

From the spectral fitting of X 1822–371 we obtained that a fraction of 71% of the Comptonization spectrum is absorbed by an excess of matter. We suppose that this matter is close to the equatorial plane, at the outer rim of the disk. Considering the area of the ADC,  $A_{ADC} = 4\pi R_c^2$ , and the area of the covered region as  $A_{cov} = 4\pi R_c h$ , where  $h$  is the height of the absorbing matter above the disk, we can write:

$$\frac{A_{cov}}{A_{ADC}} = \frac{h}{R_c} \simeq 0.71. \quad (1)$$

From this equation we obtain that the angle subtended by the absorbing region is  $\theta \sim 16^\circ$ , adopting the disk radius reported above. This scenario is in agreement with the lack of any soft component in our spectral deconvolution. In fact the inner region could be either reprocessed by the optically thick ADC or absorbed by the excess of matter at the outer accretion disk originating the partial covering.

Having the temperature of the seed photons for the Comptonization, we can derive the radius of the seed-photon emitting region. Following in’t Zand et al. (1999), this radius can be expressed as  $R_W = 3 \times 10^4 D [f_{bol} / (1 + y)]^{1/2} / (kT_0)^2$  km, where  $D$  is the distance of the source in kpc,  $f_{bol}$  is the unabsorbed flux in  $\text{ergs cm}^{-2} \text{ s}^{-1}$ ,  $kT_0$  is the seed photon temperature in keV, and  $y = 4kT_e \tau^2 / m_e c^2$  is the relative energy gain due to the Comptonization. We obtained from the fit an upper limit for the seed-photon temperature (see Table 1, Model 4). Using this upper limit in the formula above

we obtain a lower limit for the seed-photon radius of  $\sim 24$  km. We can suppose that these photons come from the inner region of the system, as the neutron star or the boundary layer between the neutron star and the accretion disk, the inner radius of the accretion disk or both these regions.

Another component of the model is an emission line at 6.5 keV with an equivalent width of  $\sim 150$  eV. This is probably due to fluorescence of moderately ionized iron. A possible origin of the emission line could be Compton reflection of the photons from the ADC by the accretion disk (George & Fabian 1991; Matt, Perola, & Piro 1991). However, the large value of the equivalent width seems to be incompatible with this interpretation. In fact, for inclinations larger than  $80^\circ$ , the iron line equivalent width should have a value of  $\sim 20$  eV (Brandt & Matt, 1994). Moreover the iron line equivalent width has a maximum value of  $\sim 130$  eV for an isotropic source covering half of the sky ( $\Omega/2\pi = 1$ ) as seen by the reflector and with an inclination angle of the system  $i = 0$ . On the other hand there are indications suggesting that the emission line in X 1822–371 originates in the ADC. In fact, according to Vrtilik et al. (1993), when the iron emission line originates in ADC, its equivalent width increases with increasing the inclination angle  $i$ : for  $i \sim 80^\circ$  the equivalent width is  $\sim 150$  eV (see Fig. 6 in Vrtilik et al., 1993). This is in agreement with our results for X 1822–371, for which we obtain an equivalent width of the emission iron line of  $\sim 150$  eV for  $i \sim 85^\circ$  (the inclination angle of X 1822–371). Note that the ADC origin (instead of the disk origin) of the iron line is also in agreement with our spectral modelling of the continuum, in which the emission from the accretion disk is not directly observed.

The iron line we observe in X 1822–371 is quite broad ( $\sim 0.7$  FWHM). Since we have excluded a disk origin for this line we cannot explain its broadening with the standard scenario adopted for Active Galactic Nuclei (AGN) containing massive black holes, where the broadening of the iron line is thought to be the result of general relativistic effects in the innermost regions of an accretion disk. In the case of coronal origin of the iron line, its width can be explained by Compton scattering of the line photons in the optically thick plasma surrounding the central X-ray source. This produces a genuinely broad gaussian distribution of line photons, with  $\sigma \gtrsim E_{Fe}(kT_e/m_e c^2)^{1/2}$ , where  $E_{Fe}$  is the centroid energy of the iron line and  $kT_e$  is the electron temperature in the ADC. More detailed calculations, in which the dependence on the optical depth is taken into account, show that this effect can explain the width of the iron line for temperatures of the emitting region of a few keV (Kallman & White 1989, see also Brandt & Matt 1994). The presence of several unresolved components from many iron ionization stages (line blending) can also contribute to the line broadening. In this case the single components could be resolved by the new high resolution instruments on board of Chandra and *XMM-Newton*. The observation of a broad iron line whose width cannot be explained by relativistic Doppler effects in the innermost region of an accretion disc is interesting and suggests alternative explanations, the most probable of which being Comptonization, for the line broadening in LMXBs. However, it is important to observe that Comptonization fails to explain the shape of the line in AGNs, for which the most probable broadening mechanism is relativistic Doppler effects (e.g. Ruszkowski et al. 2000; Misra 2001).

We observe another emission line at  $\sim 1.9$  keV with an equivalent width of  $\sim 54$  eV. This line



could be due to emission from the L-shell of ionized iron (Fe XXIII-XXIV for plasma densities of  $\sim 10^{11} \text{ cm}^{-3}$ , see Kallman et al., 1996) or from the K-shell of highly ionized Si or Mg. The emission region of this line could be the outer region of the ADC at high latitude ( $> 15^\circ$ ) where the coronal density is expected to be around  $10^{11} - 10^{12} \text{ cm}^{-3}$  (Vrtilek et al., 1993). The last component is an absorption edge at  $\sim 8.7 \text{ keV}$  with an optical depth of  $\sim 0.1$ . Following Turner et al. (1992) for a correspondence between iron edge energy and ionization level, this edge corresponds to Fe XXIV. This confirms the idea of highly ionized material present around the compact object. The best fit value for the optical depth  $\tau_{edge}$ , considering the photoionization cross section for the K-shell of Fe XXIV (Krolik & Kallman, 1987), corresponds to a hydrogen column density of  $\sim 1.3 \times 10^{23} \text{ cm}^{-2}$ , assuming cosmic abundance of iron. This is two order of magnitude higher than the measured Galactic absorption and one order of magnitude higher than the neutral matter responsible of the partial covering (see Tab. 1, Model 3 and Model 4). From the estimation of the coronal density  $N_e$  reported above, we can derive the corresponding hydrogen column density in the ADC, that is roughly  $2 \times 10^{25} \text{ cm}^{-2}$ . This suggests that a part of the ADC could be (photo) ionized and responsible for the presence of both the iron edge and the low energy emission line.

#### 4. Conclusions

We analysed data from a BeppoSAX observation of X 1822–371 performed in 1997 September 9 and 10. The energy spectrum is well described by a Comptonized spectrum with partial covering, two iron emission lines and an absorption edge. The Comptonized spectrum is probably produced in the ADC, with electron temperature of  $\sim 4.7 \text{ keV}$  and with moderate optical depth ( $\tau \sim 14$  for a spherical geometry). The partial covering could be due to an excess of neutral matter placed close to the equatorial plane at the outer rim of the accretion disk, forming a thickened outer disk subtending an angle of  $\sim 16^\circ$  as seen from the neutron star. The high inclination of the source ( $\sim 85^\circ$ ) and the presence of the cloud of neutral matter above the accretion disk does not allow to observe the direct emission from the neutron star and the inner accretion disk. In the spectrum an iron emission line is present at  $\sim 6.5 \text{ keV}$  with a large equivalent width of  $150 \text{ eV}$ . We showed that this line cannot come from the accretion disk but it is probably produced in the ADC. Another emission line at  $\sim 1.9 \text{ keV}$ , with an equivalent width of  $54 \text{ eV}$ , and an absorption edge at  $\sim 8.7 \text{ keV}$  are also detected in the spectrum, which could be produced in an ionized region in the ADC.

This work was supported by the Italian Space Agency (ASI), by the Ministero della Ricerca Scientifica e Tecnologica (MURST).

## REFERENCES

- Balucinska-Church, M., Humphrey, P. J., Church, M. J., Parmar, A. N., 2000, *A&A*, 360, 583
- Boella G., Butler R. C., Perola G. C., Piro L., Scarsi L., Blecker J., 1997, *A&AS*, 122, 299
- Brandt, W. N., Matt, G., 1994, *MNRAS*, 268, 1051
- Cottam, J., Kahn, S. M., Brinkman, A. C., den Herder, J. W., Erd, C. 2001, *A&A*, 365, L277
- Frank, J., King, A. R., Lasota, J.-P. 1987, *A&A*, 178, 137
- George I. M., & Fabian A. C., 1991, *MNRAS*, 249, 352
- Hakkila J., Myers J. M., Stidham B. J., Hartmann D. H., 1997, *AJ*, 114, 2043
- Heinz, S., & Nowak, M. A., 2001, *MNRAS*, 320, 249
- Hellier, C., and Mason, K. O., 1989, *MNRAS*, 239, 715
- Hellier, C., Mason, K. O., and Williams, O. R., 1992, *MNRAS*, 258, 457
- Kallman, T. R., Liedahl, D., Osterheld, A., & Goldstein, W., 1996, *ApJ*, 465, 994
- Kallman, T., & White, N.E., 1989, *ApJ*, 341, 955
- Ko, Y., & Kallman, T., 1994, *ApJ*, 431, 273
- Krolik, J. H., Kallman T. R., 1987, *ApJL*, 320, L5
- Mason K. O., Cordova F. A., 1982, *ApJ*, 262, 253
- Matt G., Perola G. C., Piro L., 1991, *A&A*, 247, 25
- Misra, R. 2001, *MNRAS*, 320, 445
- Parmar A. N., Oosterbroek T., Del Sordo S., Segreto A., Santangelo A., Dal Fiume D., Orlandini M., 2000, *A&A*, 356, 175
- Predehl P. & Schmitt J. H. M. M., 1995, *A&A*, 293, 889
- Ruszkowski, M., Fabian, A. C., Ross, R. R., Iwasawa, K. 2000, *MNRAS*, 317, L11
- Smale, A. P., Church, M. J., Balucinska-Church, M., [astro-ph/0010397](https://arxiv.org/abs/astro-ph/0010397)
- Sunyaev R. A., & Titarchuk L., 1980, *A&A*, 8,121
- Titarchuk L., 1994, *ApJ*, 434, 570
- Turner, T. J., Done, C., Mushotzky, R., Madejski G., 1992, *ApJ*, 391, 102

Vrtilek S. D., Soker N., Raymond J. C., 1993, ApJ, 404, 696

White N. E., & Holt S. S., 1982, ApJ, 257, 318

TABLE

Table 1: Results of the fit of the X 1822–371 spectrum in the energy band 0.12–200 keV. Uncertainties are at the 90% confidence level for a single parameter. The blackbody normalization ( $N_{\text{BB}}$ ) is in units of  $L_{37}/D_{10}^2$ , where  $L_{37}$  is the luminosity in units of  $10^{37}$  ergs/s and  $D_{10}$  is the distance to the source in units of 10 kpc.  $kT_0$  and  $kT_e$  are the seed-photon temperature and the electron temperature respectively,  $\tau$  is the optical depth of the scattering cloud. The Comptt and Compst normalization,  $N_{\text{comp}}$ , are defined as in XSPEC v.10.  $N_{\text{HPC}}$  indicates the column absorption of the partial covering and  $f$  the covering fraction.  $f_{\text{bol}}$  is the unabsorbed flux in the 0.1–100 keV range of the Comptonized component in units of ergs  $\text{cm}^{-2} \text{s}^{-1}$ .  $EQW_{\text{Fe}}$  indicates the equivalent width of the line at 6.5 keV,  $E_{\text{Fe}}$  its centroid and  $I_{\text{Fe}}$  its intensity in units of photons  $\text{cm}^{-2} \text{s}^{-1}$ ;  $EQW_{\text{LE}}$ ;  $E_{\text{LE}}$  and  $I_{\text{LE}}$  are the same parameters for the low-energy line at 1.9 keV.  $E_{\text{edge}_1}$  indicates the energy of the absorption edge at low energy and  $\tau_{\text{edge}_1}$  its relative optical depth,  $E_{\text{edge}_h}$  and  $\tau_{\text{edge}_h}$  are the same parameters for the edge at high energy.

Parameter	Model 1	Model 2	Model 3	Model 4
	BB + Comptt + Line + Edge	PC + Compst + Line	PC + Compst + Line+Line+Edge	PC + Comptt + Line+Line+Edge
$N_{\text{H}} (\times 10^{21} \text{ cm}^{-2})$	$0.62 \pm 0.20$	$1.43 \pm 0.18$	$1.23^{+0.16}_{-0.14}$	$1.09^{+0.26}_{-0.51}$
$N_{\text{HPC}} (\times 10^{22} \text{ cm}^{-2})$	–	$4.31 \pm 0.27$	$4.45 \pm 0.26$	$4.37 \pm 0.31$
$f$	–	$0.688 \pm 0.013$	$0.712 \pm 0.016$	$0.715^{+0.027}_{-0.022}$
$kT_{\text{BB}}$ (keV)	$1.590 \pm 0.041$	–	–	–
$N_{\text{BB}}$	$0.273 \pm 0.014$	–	–	–
$kT_0$ (keV)	$0.133^{+0.033}_{-0.038}$	–	–	$< 0.20$
$kT_e$ (keV)	$4.526^{+0.067}_{-0.065}$	$4.802^{+0.069}_{-0.067}$	$4.724 \pm 0.075$	$4.711 \pm 0.075$
$\tau$	$24.22^{+0.37}_{-0.92}$	$13.52 \pm 0.26$	$13.81 \pm 0.35$	$14.61 \pm 0.37$
$N_{\text{comp}} (\times 10^{-2})$	$2.09^{+0.21}_{-0.13}$	$7.71 \pm 0.30$	$7.67 \pm 0.36$	$6.22^{+3.88}_{-1.10}$
$f_{\text{bol}}$	$0.98 \times 10^{-9}$	$1.53 \times 10^{-9}$	$1.55 \times 10^{-9}$	$1.49 \times 10^{-9}$
$E_{\text{Fe}}$ (keV)	$6.528 \pm 0.046$	$6.523 \pm 0.055$	$6.521 \pm 0.050$	$6.520 \pm 0.050$
$\sigma_{\text{Fe}}$ (keV)	$0.292^{+0.065}_{-0.062}$	$0.444^{+0.119}_{-0.086}$	$0.302^{+0.075}_{-0.068}$	$0.303^{+0.075}_{-0.068}$
$I_{\text{Fe}} (\times 10^{-3})$	$0.95 \pm 0.14$	$1.37^{+0.23}_{-0.19}$	$0.97 \pm 0.15$	$0.97^{+0.17}_{-0.14}$
$EQW_{\text{Fe}}$ (eV)	$158 \pm 23$	$222^{+37}_{-31}$	$153 \pm 25$	$152^{+26}_{-22}$
$E_{\text{LE}}$ (keV)	–	–	$1.968^{+0.050}_{-0.061}$	$1.961^{+0.052}_{-0.072}$
$\sigma_{\text{LE}}$ (keV)	–	–	$0.116^{+0.083}_{-0.087}$	$0.124^{+0.093}_{-0.087}$
$I_{\text{LE}} (\times 10^{-3})$	–	–	$1.54^{+0.82}_{-0.54}$	$1.64^{+1.11}_{-0.62}$
$EQW_{\text{LE}}$ (eV)	–	–	$53^{+28}_{-18}$	$57^{+38}_{-21}$
$E_{\text{edge}_1}$ (keV)	$1.315 \pm 0.056$	–	–	–
$\tau_{\text{edge}_1}$	$0.325^{+0.077}_{-0.070}$	–	–	–
$E_{\text{edge}_h}$ (keV)	–	–	$8.69^{+0.24}_{-0.20}$	$8.69^{+0.24}_{-0.20}$
$\tau_{\text{edge}_h}$	–	–	$0.097 \pm 0.029$	$0.097 \pm 0.029$
$\chi^2/\text{d.o.f.}$	245/201	291/204	206/199	206/198

FIGURES

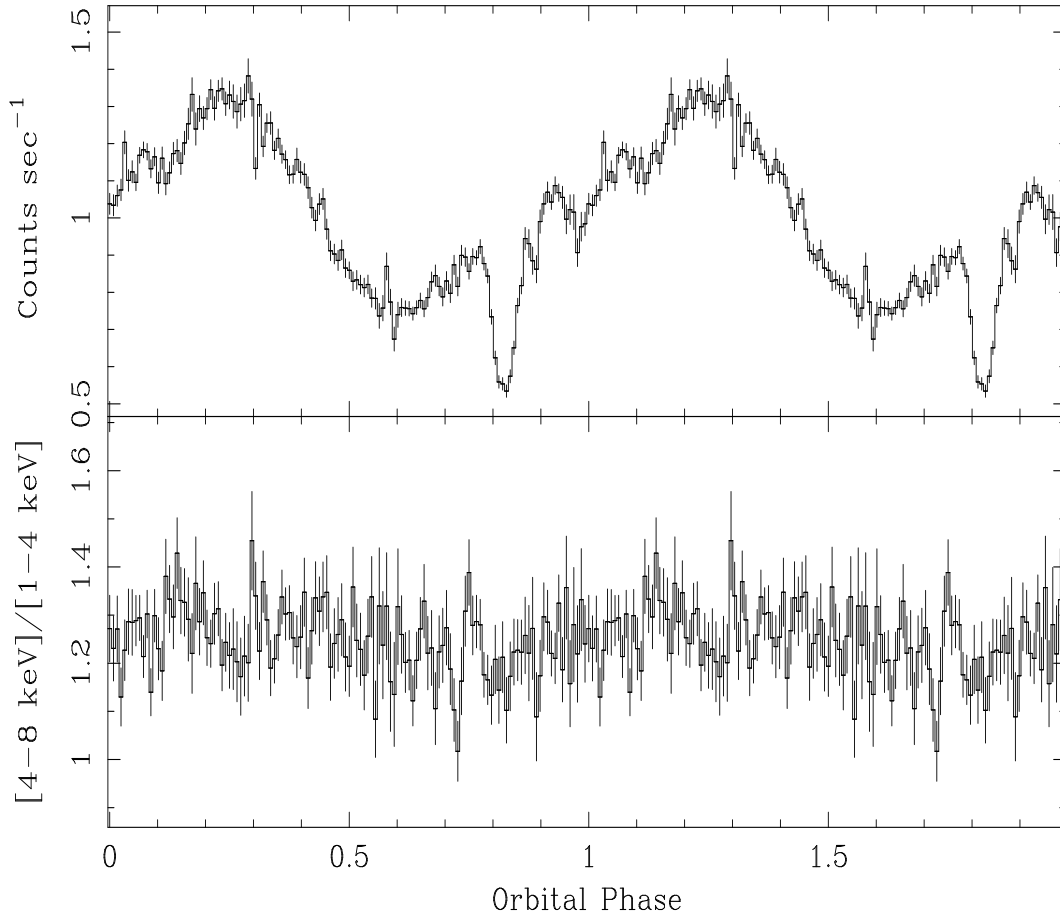


Fig. 1.— Upper panel: folded light curve of X 1822–371 in the energy band 1.8–10 keV (MECS data) vs. the orbital phase. Lower panel: The ratio of the count rate in the energy band 4–8 keV with respect to that in 1–4 keV vs. the orbital phase. Two orbital phases are shown for clarity.

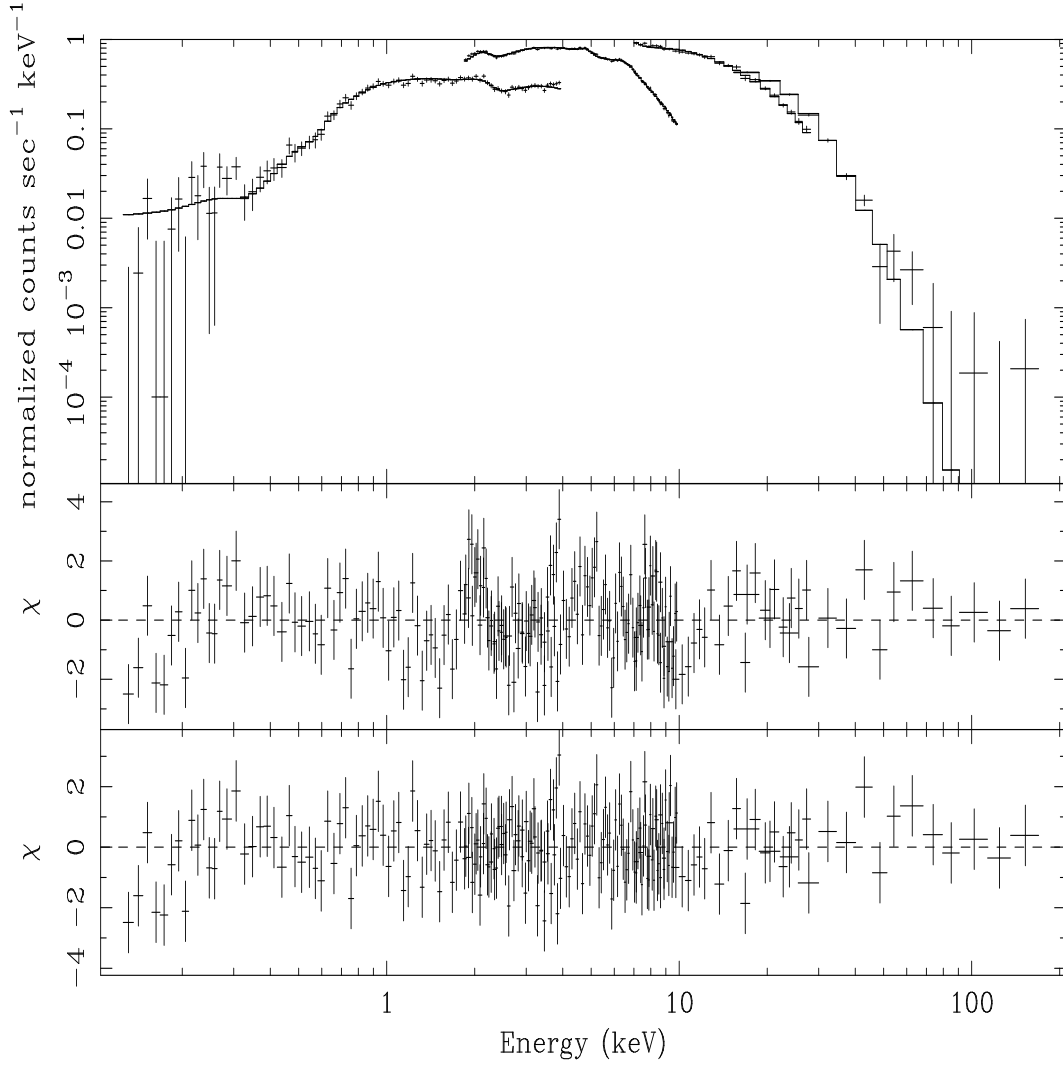


Fig. 2.— Energy spectra (0.1–200 keV) of X 1822–371. Data and the Model 2 (see Tab. 1) are shown in the upper panel, residuals in units of  $\sigma$  with respect to the Model 2 are shown in the middle panel. In the lower panel the residuals in units of  $\sigma$  with respect to the best fit model (Model 3) are shown.

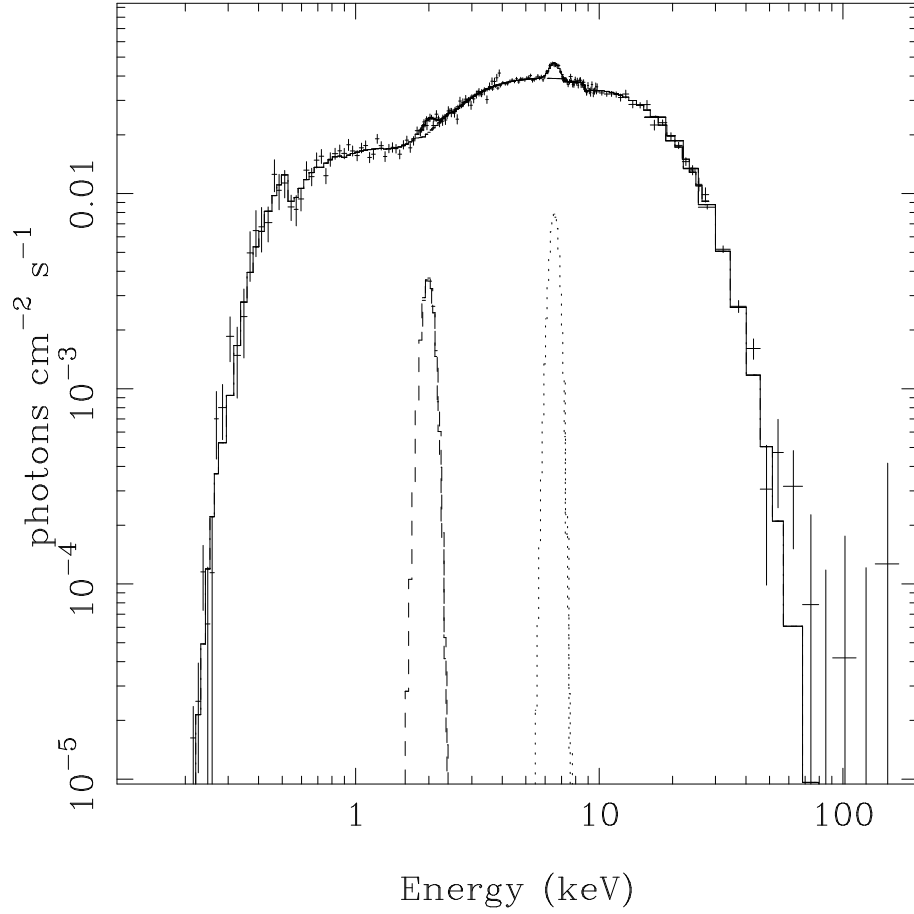


Fig. 3.— Unfolded spectrum of X 1822–371 and the best fit model (Model 3). The single components of the model are also shown. The solid line is the *Compt* model with partial covering. The low-energy line at  $\sim 1.9$  keV (dashed line) and the iron emission line at  $\sim 6.5$  keV (dotted line) are also shown. The absorption edge at 8.7 keV is visible.